Kovove Mater. 61 2023 115–120
DOI: 10.31577/km.2023.2.115

Effect of arc remelting on microstructure and pitting corrosion resistance of 441 ferritic stainless steel

Shuangchun Zhu[1]*, Baosen Wang[2], Biao Yan[3]

[1] *Jiangsu College of Engineering and Technology, 226006 Nantong, P. R. China*
[2] *Central Research Institute, Baoshan Iron & Steel Co., Ltd., 201900 Shanghai, P. R. China*
[3] *School of Material Science and Engineering, Tongji University, 201804 Shanghai, P. R. China*

Received 15 December 2022, received in revised form 14 February 2023, accepted 16 February 2023

Abstract

In this paper, the large area plate of arc-remelted metal of 441 ferritic stainless steel is prepared by multi-arc remelting. The pitting corrosion resistance of base metal and arc-remelted metal is compared through the pitting corrosion immersion test. The microstructure changes of 441 ferritic stainless steel after arc remelting and its influence on pitting corrosion resistance are studied through metallographic structure observation, precipitate analysis and corrosion pit surface observation and analysis. The results show that, compared with the base metal, the grains of arc remelted metal structure grow abnormally and form coarse ferrite columnar structure; there are large particles of carbonitride precipitates of Ti and Nb, and small particles of Laves precipitates containing Nb in the base metal, and the precipitates in the arc remelted metal are smaller and more evenly distributed, most of which are composite precipitates of Nb and Ti. The corrosion rate of base metal is 23.4 $\mathrm{g\,m^{-2}\,h^{-1}}$. After arc remelting, the corrosion rate of metal is 20.88 $\mathrm{g\,m^{-2}\,h^{-1}}$, and the pitting corrosion resistance is improved.

K e y w o r d s: 441 ferritic stainless steel, pitting corrosion, arc remelting, precipitate

1. Introduction

Compared with austenitic stainless steel, ferritic stainless steel not only has excellent corrosion resistance [1, 2], and it does not contain Ni with an unstable and high price [3], but also has lower cost, lower expansion coefficient and higher thermal conductivity [4, 5], which is widely used in automobile exhaust system [6, 7]. As a part exposed under the automobile chassis, the automobile exhaust not only contacts the automobile exhaust and its condensate but also inevitably contacts with other corrosive media in the external environment, especially the ground snow melting salt in winter. Therefore, ferritic stainless steel for automobile exhaust systems also needs good corrosion resistance [8–10].

It is well known that Cr is the main element to ensure the corrosion resistance of stainless steel, and its content profoundly impacts the corrosion properties of stainless steel. Arshad Yazdanpanah et al. [11] found that the change of Cr content in AISI304 within the range of standard designations will also affect the corrosion properties of stainless steel, AISI304 with lower Cr content is more sensitive to pitting corrosion and stress corrosion cracking. In addition to Cr, other elements will also affect the corrosion properties of stainless steel. For example, C and N will cause grain boundary Cr depletion and cause intergranular corrosion. Modern ferritic stainless steel solves the problem of grain boundary sensitization by reducing the content of C and N and adding stabilizing elements Ti and Nb. Combining Ti and Nb with C and N, the carbonitride of Ti and Nb is formed, which reduces the Cr deficiency at the grain boundary caused by the precipitation of chromium carbide and improves the intergranular corrosion resistance of ferritic stainless steel [12–14]. In addition to chemical composition, the corrosion characteristics of steel are also closely related to the microstructure of steel, which provides another way to improve the corrosion resistance of steel.

*Corresponding author: e-mail address: zhushuangchun@tju.edu.cn

Table 1. Chemical constituents of test materials

Element	C	Si	Mn	P	S	Cr	Nb	N	Ti
Mass fraction (%)	0.005	0.38	0.34	0.008	0.002	18.63	0.43	0.008	0.14

M. Franceschiet et al. [15] studied a novel high silicon austempered (AHS) steel and investigated the effect of different austenitizing temperatures on the final microstructure in the entire austenitic and biphasic regime. The results showed that due to the low residual stress, the corrosion resistance of the sample would increase with the increase of the volume fraction of residual austenite. Due to the large grain size and the change of precipitated phase after welding of ferritic stainless steel [16], it is bound to impact the corrosion resistance. The pipe welding of automobile exhaust systems generally adopts the self-melting welding of a cold-rolled plate of ferritic stainless steel. The welding area is narrow, so it is difficult to test and evaluate the performance of the welding area separately. To determine the effect of microstructure change on the corrosion resistance of ferritic stainless steel after welding, a large area of microstructure material after self-melting welding is obtained by multi-arc remelting to study the effect of microstructure change after welding on the pitting corrosion resistance of the material. The results showed that the pitting resistance of 441 ferritic stainless steel could be improved by arc remelting because the large precipitates in the base metal were dissolved after arc remelting.

2. Experimental method

The test plate is a cold-rolled annealed plate of 441 ferritic stainless steel with a thickness of 1.5 mm. The chemical composition is shown in Table 1.

Five overlapping self-melting arc remelting processes were carried out on the cold-rolled plate using tungsten argon arc welding (TIG), forming 441 ferritic stainless steel arc remelting weld beads with a width > 25 mm, see Fig. 1. The welding current was 80 A, the welding voltage was 11 V, the welding speed was 150 mm min^{-1}, the welding shielding gas and a back shielding gas were 99.999 % high-purity Ar gas, and the shielding gas flow of both was set to 12 L min^{-1}.

The corrosion immersion samples were cut from the base metal and arc-remelted metal of 441 ferritic stainless steel by wire-electrode cutting, as shown in Fig. 1 (b), and the sample size was 25 mm × 20 mm × 1.0 mm. Two parallel samples were ground from each group, the six surfaces of each sample were ground with 600 # sandpaper, washed with absolute ethanol and blown dry, then weighed. The electronic balance used for weighing was *Mettler Toledo xp504*, and the weighing accuracy was 0.1 mg.

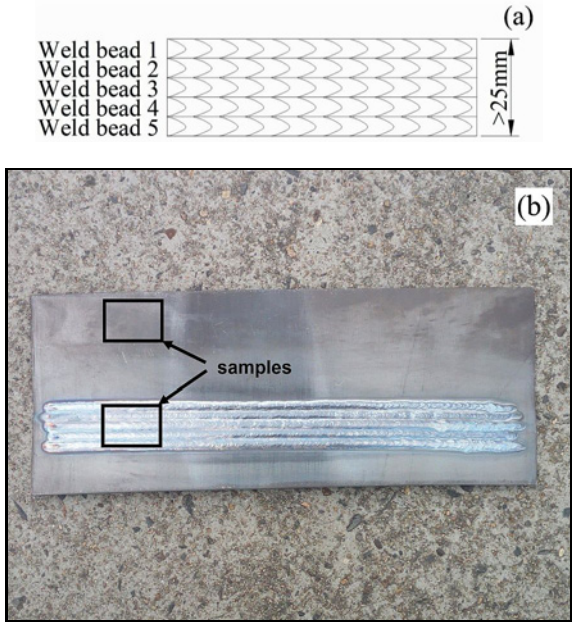

Fig. 1. Distribution of weld bead in cold rolled sheet: (a) sketch, (b) photo.

The pitting corrosion immersion test was carried out according to GB/t17897-1999. The immersion solution was a 6 % ferric chloride hydrochloric acid solution, and the test temperature was set to 35 ± 1 ℃; the base metal and the remelted metal were tested with two samples, respectively. The sample was taken out after 24 h of continuous immersion, and the corrosion products on the sample were removed, washed with an ultrasonic wave and weighed after drying.

The calculation formula of corrosion weight loss rate X is as follows:

$$X = \frac{W_{\mathrm{F}} - W_{\mathrm{B}}}{St}, \tag{1}$$

where W_{F} is the weight of the sample before corrosion, W_{B} is the weight of the sample after corrosion, S is the total surface area of the sample, and t is the immersion corrosion time.

According to the observation requirements of the cross-section of the arc remelting weld bead and the cross-section of the base metal, the metallographic samples of the remelted metal and the base metal were cut. After grinding and polishing, ferric chloride solution ($FeCl_3 : HCl : H_2O$ = 5g : 50 ml : 100 ml) was used as a metallographic etchant for corrosion, and

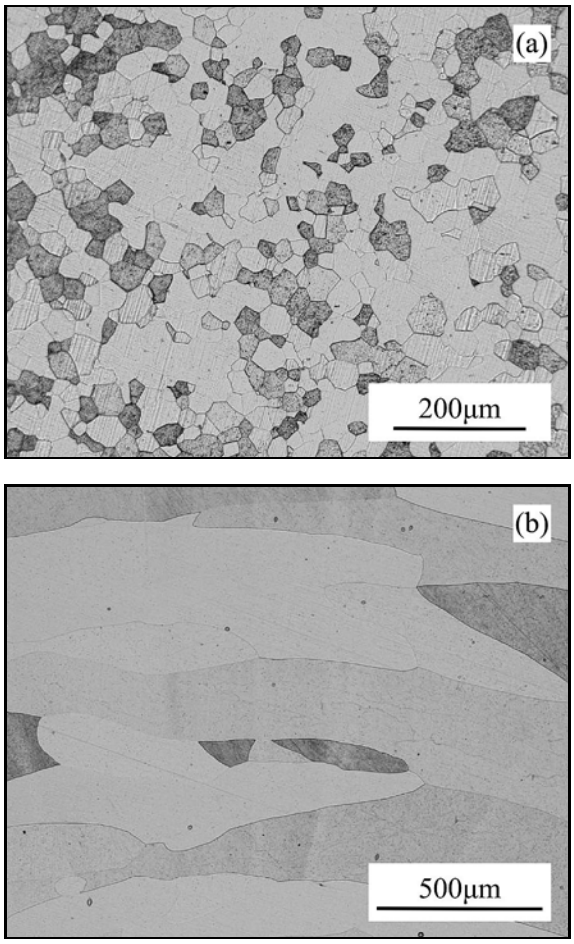

Fig. 2. Metallography of 441 ferritic stainless steel: (a) base metal and (b) remelting metal.

then the samples were washed with water and absolute ethanol, then dried. The metallographic optical microscope (*Leica microsystems dm6000m*) was used to observe the metallographic structure, and the scanning electron microscope (*Zeiss Evo ma25*) was used to observe the metallographic structure and the surface of the corrosion pit. The composition of the precipitated phase was analyzed by the energy spectrometer (*Oxford Instruments X-MAX*) attached to the scanning electron microscope.

3. Experimental results and analysis

3.1. Metallographic structure

Figure 2 shows cross-sectional metallographic photographs of the base metal and the arc-remelting metal of ferritic stainless steel. The structure of the base metal of ferritic stainless steel is shown as refined equiaxed ferrite grains. Still, after the action of arc heat, the grains of the arc-remelting weld bead grow

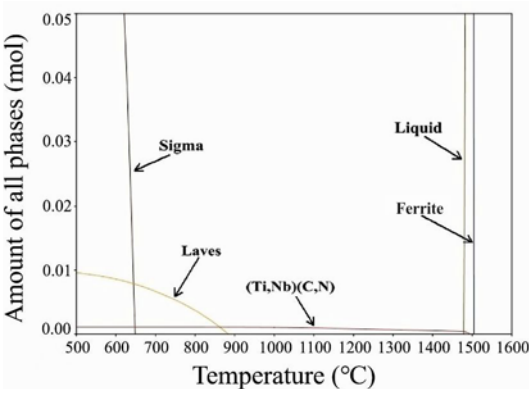

Fig. 3. Equilibrium phase diagram of 441 ferritic stainless steel calculated by *Thermo-calc Software.*

abnormally. The grain growth direction is opposite to the heat dissipation direction on both sides of the remelting weld bead, forming a coarse columnar crystal structure.

3.2. Precipitated phase

According to the chemical composition of 441 ferritic stainless steel in Table 1, Thermo-calc software was used to calculate the relationship between the mole fraction of the precipitated phase and temperature in the thermodynamic equilibrium state of the material. As shown in Fig. 3, the solidification starting temperature of 441 stainless steel is about 1510 ℃, and the precipitated phases mainly include carbonitrides of Ti and Nb, Laves phase, and σ phase. Among these precipitates, the precipitation temperature of carbonitrides of Ti and Nb is higher, which can be formed in the solid-liquid coexistence stage near 1500 ℃, and the precipitation temperature of Laves phase is near 890 ℃, the initial precipitation temperature of σ phase is about 650 ℃.

Figure 4a is an SEM observation of the distribution of precipitates in the base metal of 441 ferritic stainless steel. Precipitates can be observed in the grain interior and boundary of the base metal, and there are two types of precipitates: small and large. There are also some differences in the distribution of precipitates. The number of fine precipitates is large, and the distribution is relatively fractional, and most of them are Laves precipitates rich in Nb. The EDS analysis results of large particle precipitates are shown in Fig. 4b. Referred to the calculation results of *Thermo-calc software*, it can be inferred that the precipitates of large particles are mainly TiN precipitates and composite carbonitride precipitates of Ti and Nb adsorbed on the previously precipitated TiN particles.

Figure 5 shows the distribution of precipitates in the arc-remelted metal of 441 ferritic stainless steel. Compared with the base metal, there is no large gran-

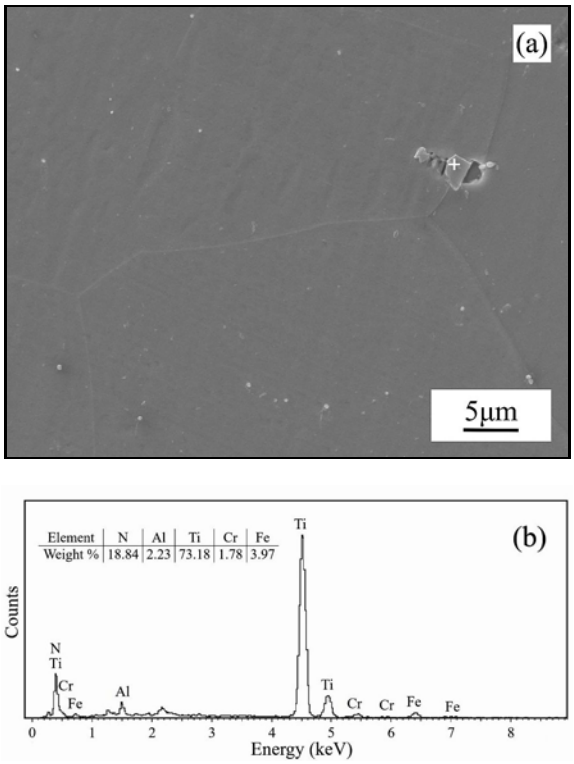

Fig. 4. Precipitated phases in base metals: (a) SEM and (b) EDS.

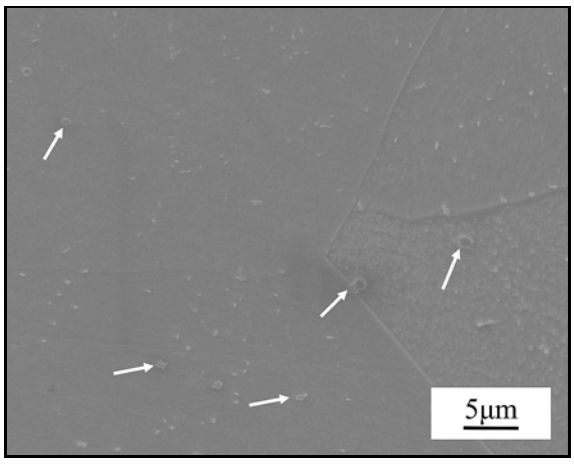

Fig. 5. Distribution of precipitates in remelted metal.

ular precipitate in the remelting metal. The precipitates show the characteristics of large quantity, small size and uniform distribution, which is closely related to the characteristics of the arc-remelting process. The arc-remelting process is a process of rapid heating and cooling. The remelted metal cools rapidly from the liquid state to the solid state. Therefore, the solute atoms have no time to diffuse in the matrix, which inhibits the growth of precipitates in the metal so that the

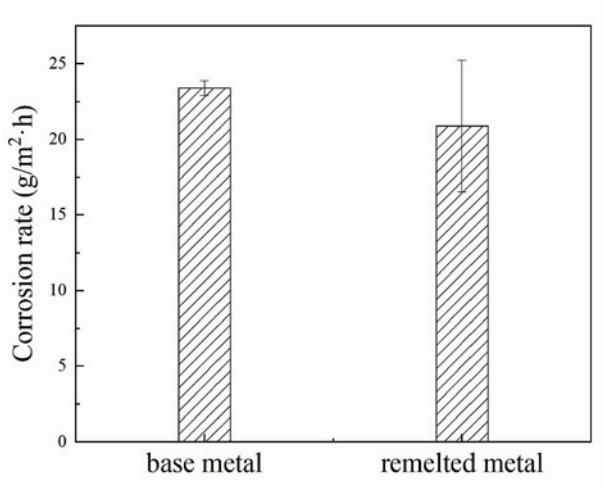

Fig. 6. Corrosion rate of pitting corrosion immersion test of 441 ferritic stainless steel.

precipitates in the remelted metal are relatively evenly nucleated in the matrix, and the growth process is hindered. Therefore, the metallographic structure shows many dispersed and fine precipitate distribution characteristics when cooled to room temperature.

These precipitates are relatively complex, including carbonitrides of Nb and Ti, oxides of Ti, etc., compared with the base metal, there are no large TiN particles. Ti, generally together with Nb, forms small-size composite carbides of Ti and Nb, and small-size carbonitrides of Ti can also be observed. In addition, due to the difference in gas protection effect in the welding process, air entrainment in the weld is possible, resulting in oxygen infiltration into the weld, and oxide of Ti inclusions is formed in the weld.

3.3. Pitting corrosion resistance

Figure 6 shows the corrosion rate (weight loss rate) of base metal samples and arc-remelted metal samples of 441 ferritic stainless steel after pitting corrosion immersion. The corrosion rate of base metal is $23.4\,\mathrm{g\,m^{-2}\,h^{-1}}$, and the corrosion rate of remelting metal is $20.88\,\mathrm{g\,m^{-2}\,h^{-1}}$. It can be seen that the pitting corrosion resistance of stainless steel is improved after arc remelting.

From the microstructure perspective, inclusions, intermetallic compounds and grain boundaries in stainless steel are the starting positions that easily cause pitting corrosion. 441 ferritic stainless steel contains Ti and Nb elements. Ti and Nb have a strong affinity with C elements, which can stabilize C elements in stainless steel, inhibit the generation of carbides of Cr, prevent deficiency of Cr at the grain boundary, which can lead to grain boundary corrosion sensitivity, and reduce the intergranular corrosion resistance of ferritic stainless steel. However, there

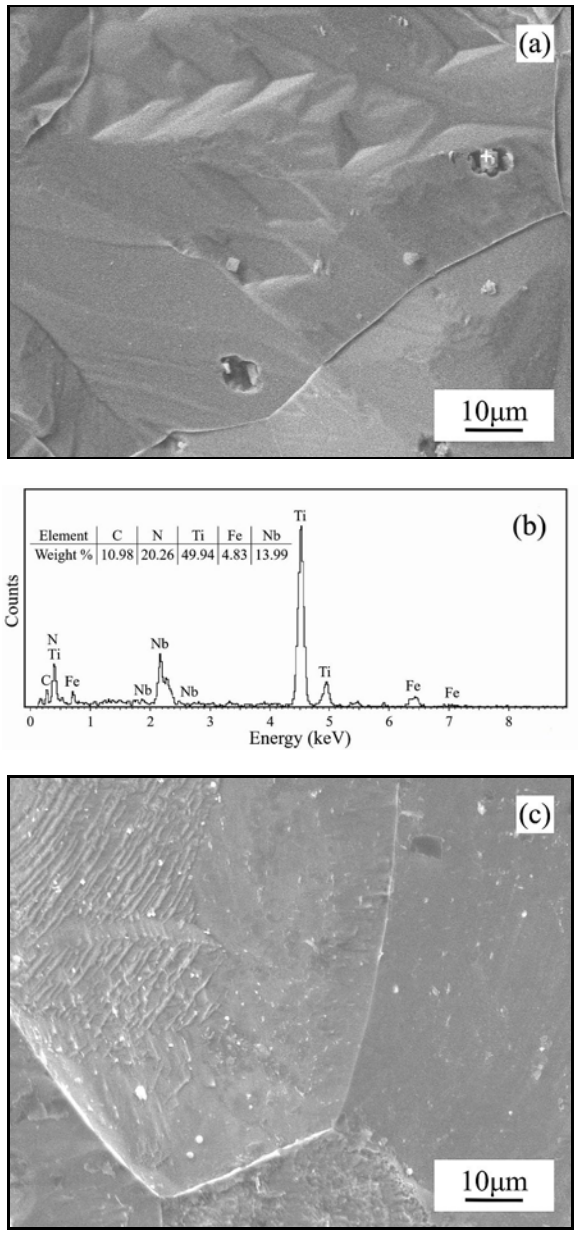

Fig. 7. SEM photos and EDS analysis of precipitates on corrosion surface of 441 stainless steel after pitting corrosion immersion test: (a) base metal, (b) EDS analysis of precipitates on corrosion surface of base metal, and (c) arc remelted metal.

will be Cr segregation around the carbonitride precipitates of Ti and Nb to form Cr compounds, resulting in Cr-poor areas around them, leading to pitting corrosion [17]. In particular, the large particle precipitates of TiN in the base metal of 441 ferritic stainless steel are an important pitting source of high-purity ferritic stainless steel [18], while the precipitates in the arc remelted metal of 441 ferritic stainless steel have a small size and uniform distribution, which contribute less to pitting corrosion, thus improving the pitting corrosion resistance.

Figures 7a–c are SEM photos of the surface of the corrosion pit after the pitting immersion test of base metal and arc-remelted metal of 441 ferritic stainless steel, and the energy spectrum analysis results of its precipitates. It can be seen from these photos that there are large particles of TiN on the surface of 441 base metal corrosion pit, and small corrosion pits have been formed around large particles of TiN, which has become the origin of pitting corrosion, which proves that the TiN precipitates of large particles are the cause of pitting corrosion. For the remelted metal sample of 441 ferritic stainless steel, many fine precipitates appear on the corrosion surface after pitting immersion, most of which are complex precipitates of Ti and Nb. However, these particles are closely combined with the surrounding matrix, and their contribution to pitting corrosion is less than that of large particles of TiN precipitates so that the pitting corrosion resistance of remelted metal of ferritic stainless steel is better than that of base metal of ferritic stainless steel. Therefore, we can find that 441 ferritic stainless steel contains stabilizing elements of Nb and Ti. The remelted metal solidifies and cools rapidly during arc remelting so that the carbonitride precipitation of Nb and Ti is dispersed, and the size is small, which has little effect on pitting corrosion. In addition, because the grain boundary is also the location where pitting corrosion is easy to occur, the abnormal coarsening of the grains of remelted metal reduces the grain boundary, which also reduces the pitting corrosion sensitivity to a certain extent.

4. Conclusions

1. The microstructure of the base metal of 441 ferritic stainless steel is fine equiaxed ferrite grains. After arc remelting, the ferrite grains grow abnormally and form coarse ferrite columnar structure.

2. There are two sizes of precipitates in the base metal of 441 ferritic stainless steel. The precipitates of large particles are mainly precipitates of TiN, and the precipitates of small particles are mostly Laves precipitates containing Nb. The precipitates in the arc-remelted metal of 441 ferritic stainless steel are small and evenly distributed, and most of them are the composite precipitates of Nb and Ti.

3. The corrosion rate of 441 ferritic stainless steel base metal is $23.4\,\mathrm{g\,m^{-2}\,h^{-1}}$. After arc remelting, the metal corrosion rate is $20.88\,\mathrm{g\,m^{-2}\,h^{-1}}$, and the pitting corrosion resistance is improved.

Acknowledgements

This work was funded by the Guiding Project of Nantong Basic Research and Livelihood Science and Technology Plan (grant No. JCZ21081) and supported by the

Teaching Reform Research Plan of Jiangsu College of Engineering and Technology (grant No. GYJY202109).

References

[1] R. Kaul, P. Ganesh, P. Tripathi, R. V. Nandedkar, A. K. Nath, Comparison of laser and gas tungsten arc weldments of stabilized 17 wt.% Cr ferritic stainless steel, Mater. Manuf. Processes 18 (2003) 563–580. https://doi.org/10.1081/AMP-120022497

[2] H. X. Zhang, H. Z. Li, Z. B. Wang, W. X. Wang, X. B. Zhang, Z. F. Yan, Effect of heat input on microstructure and mechanical properties of ultra-thin 443 ferritic stainless steel, Trans. China Weld. Inst. 4 (2013) 15–18.

[3] H. Y. Zhang, L. W. Zheng, X. M. Meng, W. Liang, Effect of electrochemical hydrogen charging on hydrogen embrittlement sensitivity of Cr15 ferritic and 304 austenitic stainless steel, Journal of Chinese Society for Corrosion and Protection 41 (2021) 202–208. https://doi.org/10.11902/1005.4537.2020.099

[4] Y. Shao, Y. M. Li, C. X. Liu, Z. S. Yan, Y. C. Liu, Annealing process optimization of high frequency longitudinal resistance welded low-carbon ferritic stainless steel pipe, Acta Metall. Sin. 55 (2019) 1367–1378. https://doi.org/10.11900/0412.1961.2019.00051

[5] A. R. Huang, W. Zhang, X. L. Wang, C. J. Shuang, J. J. Fan, Corrosion behavior of ferritic stainless steel in high temperature urea environment, Chin. J. Mater. Res. 34 (2020) 712–720. https://doi.org/10.11901/1005.3093.2020.065

[6] X. Li, J. Shu, L. Q. Chen, H. Y. Bi, Effect of cerium on high-temperature oxidation resistance of 00Cr17NbTi ferritic stainless steel, Acta Metall. Sin. (Engl. Lett.) 27 (2014) 501–507. https://doi.org/10.1007/s40195-014-0079-6

[7] X. Li, H. Y. Bi, L. Q. Chen, Effects of tungsten on the oxidation resistance and high-temperature strength of 18CrNbTi ferritic stainless steel, Baosteel Tech. Res. 10 (2016) 41–45. https://doi.org/10.3969/j.issn.1674-3458.2016.04.007

[8] W. H. Ruan, S. D. Wang, M. C. Li, J. N. Shen, Corrosion behavior of 409 ferritic stainless steel in condensate solution of automotive mufflers, Corros. Sci. Prot. Technol. 24 (2012) 301–304.

[9] T. Ujiro, M. Kitazawa, F. Togashi, Corrosion resistance of muffler materials in automotive exhaust gas condensates, Mater. Perform. 33 (1994) web.

[10] H. Y. Bi, Y. Wu, X. Li, Application and failure evaluation of ferritic stainless steels for automotive exhaust systems, Baosteel Tech. Res. 4 (2010) 10–14. https://doi.org/10.3969/j.issn.1674-3458.2010.01.002

[11] A. Yazdanpanah, L. Pezzato, M. Dabalà, Stress corrosion cracking of AISI 304 under chromium variation within the standard limits: Failure analysis implementing microcapillary method, Eng. Fail. Anal. 142 (2022) 106797. https://doi.org/10.1016/j.engfailanal.2022.106797

[12] J. Liu, X. H. Luo, X. Q. Hu, S. Liu, Effect of Ti and Nb micro-alloying on the microstructure of the ultra-purified 11% Cr ferritic stainless steels, Acta Metall. Sin. 47 (2011) 688–696. https://doi.org/10.3724/SP.J.1037.2011.00059

[13] M. X. Li, W. Zhang, X. L. Wang, E. H. Chen, C. Chen, H. W. Zhang, C. J. Shang, Effect of Nb on the performance of 409 stainless steel for automotive exhaust systems, Steel Res. Int. 89 (2018) 1700558. https://doi.org/10.1002/srin.201700558

[14] Z. H. Dong, Y. W. Li, A. Babkin, Y. L. Chang, Research status of ferritic stainless steel weld grain refinement technology, Materials Reports 36 (2022) 184–193. https://doi.org/10.11896/cldb.21040102

[15] M. Franceschi, L. Pezzato, A. G. Settimi, C. Gennari, M. Pigato, M. Polyakova, D. Konstantinov, K. Brunelli, M. Dabalà, Effect of different austempering heat treatments on corrosion properties of high silicon steel, Materials 14 (2021) 288. https://doi.org/10.3390/ma14020288

[16] I. Acar, B. Cevik, B. Gulenc, Analysis of mechanical and microstructural characteristics of AISI 430 stainless steel welded by GMAW, Kovove Mater. 60 (2022) 21–30. https://doi.org/10.31577/km.2022.1.21

[17] G. Y. Ma, H. T. Chen, Y. P. Lang, F. Rong, G. X. Li, Effect of non-metallic inclusions on pitting corrosion resistance of ferritic stainless steel 439M, J. Iron Steel Res. 27 (2015) 40–44. https://doi.org/10.13228/j.b0yuan.issn1001-0963.20140369

[18] J. H. Tian, C. Zhang, H. P. Wang, B. S. Chu, L. F. Sun, M. F. Jiang, Effect of Nb, Ti on pitting corrosion resistant of high-pure ferritic stainless steel, Proceedings of the 17th National steelmaking Academic Conference (Volume B) Hangzhou: Steelmaking Branch of The Chinese Society for Metals (2013), pp.1360–1364.